Structural Basis for Inhibition of the Histone Chaperone Activity of SET/TAF-Iβ by Cytochrome *c*

Katiuska González-Arzola[1], Irene Díaz-Moreno[1,*], Ana Cano-González[2], Antonio Díaz-Quintana[1], Adrián Velázquez-Campoy[3], Blas Moreno-Beltrán[1], Abelardo López-Rivas[2], Miguel Á. De la Rosa[1,*]

[1]IBVF-cicCartuja, University of Seville - CSIC, Avda. Américo Vespucio 49, 41092 Sevilla (Spain). [2]Centro Andaluz de Biología Molecular y Medicina Regenerativa-CSIC, CABIMER, Avda. Américo Vespucio s/n, Sevilla (Spain). [3]Institute for Biocomputation and Physics of Complex Systems (BIFI), Joint Unit Institute of Physical Chemistry "Rocasolano" (IQFR)-BIFI-Spanish National Research Council (CSIC); Department of Biochemistry and Molecular and Cellular Biology, University of Zaragoza, Zaragoza (Spain); ARAID Foundation, Zaragoza (Spain).

Submitted to Proceedings of the National Academy of Sciences of the United States of America

Chromatin is pivotal for regulation of the DNA damage process insofar as it influences access to DNA and serves as a DNA repair docking site. Recent works identify histone chaperones as key regulators of damaged chromatin's transcriptional activity. However, understanding how chaperones are modulated during DNA damage response is still challenging. This study reveals that the histone chaperone SET/TAF-Iβinteracts with cytochrome *c* following DNA damage. Specifically, cytochrome *c* is shown to be translocated into cell nuclei upon induction of DNA damage with camptothecin, but not upon stimulation of the death receptor or stress-induced pathways. Cytochrome *c* was found to competitively hinder binding of SET/TAF-Iβ to core histones, thereby locking its histone binding domains and inhibiting its nucleosome assembly activity. In addition, we have used Nuclear Magnetic Resonance spectroscopy, calorimetry, mutagenesis and molecular docking to provide an insight into the structural features of the formation of the complexbetween cytochrome *c* and SET/TAF-Iβ. Overall, these findings establish a framework for understanding the molecular basis of cytochrome *c*-mediated blocking of SET/TAF-Iβ, which subsequentlymay facilitate the development of new drugs to silence the oncogenic effect of its histone chaperone activity.

Cytochrome *c* | Histone chaperone | ITC | NMR | SET-TAF-Iβ

Introduction

The oncoprotein SET/template-activating factor (TAF)-Iβ (SET/TAF-Iβ) – also known as inhibitor-2 of protein phosphatase-2A (I_2PP2A) and inhibitor of histone acetyltransferase (INHAT) – belongs to the nucleosome assembly protein (NAP) family of histone chaperones. SET/TAF-Iβ participates in numerous of cellular processes, including cell cycle control (1), apoptosis (2), transcription regulation (3) and chromatin remodelling (4). Many recent studies highlight the chromatin-related properties of SET/TAF-Iβ. As a histone chaperone, SET/TAF-Iβ associates to core histones to shield their positive charge, preventing improper contact with DNA and facilitating the correct deposition of free histones onto DNA for nucleosome formation (5).

Recent work points to the crucial role of chromatin dynamics in DNA damage response (6-8). In fact, histone chaperones have emerged as key players in the transient disorganization of chromatin required in the DNA repair process. Thus, the histone chaperones aprataxin-PNK-like factor (APLF) (6), anti-silencing function 1 (Asf1) (9), chromatin assembly factor 1 (CAF-1) (10), death domain-associated protein 6 (DAXX) (11), facilitating chromatin transcription (FACT) (12), histone regulator A (HIRA) (13), nucleolin (14), p400 (15), nucleosome assembly protein 1-like 1 (NAP1L1) and 1-like 4 (NAP1L4) (7) are recruited to damaged chromatin, thereby promoting histone dynamics in response to DNA damage. Recently, SET/TAF-1β was found to modulate the DNA damage response by regulating chromatin compaction (16).

Recently, we have identified SET/TAF-Iβ as a target protein for cytochrome *c* (C*c*) following the release of the latter from mitochondria in human cells treated with apoptotic agents (17, 18). While it has been shown that the hemeprotein C*c* serves as an electron carrier between complexes III and IV in the mitochondrial respiratory chain, its role in nuclei has yet to be convincingly elucidated. It has been proposed, however, that C*c* accumulation in the nucleus under apoptotic stimuli relates to nuclear pyknosis, DNA fragmentation (19) and chromatin remodelling (20). Here, we show that the SET/TAF-Iβ oncoprotein interacts with C*c* in the cell nucleus in response to treatment of the cell with camptothecin (CPT), a well-known inducer of DNA damage and apoptosis, but not to treatment with other apoptosis-inducing chemical agents. We also demonstrate that C*c* impairs the histone chaperone activity of SET/TAF-Iβ through competitive binding, thereby preventing the formation of core histone-SET/TAF-Iβ complexes.

Results

Cc interacts with SET/TAF-Iβ in the nucleus in response to DNA damage

DNA damage can be induced by ionizing radiation or topoisomerase inhibitors (e.g. CPT). Subcellular localization of C*c* in Heltog cells – a HeLa cell line constitutively expressing green fluorescent protein (GFP)–tagged C*c* – showed C*c*-GFP predominantly in mitochondria of untreated cells (Fig. 1A: left). Confocal analysis of cells treated with 20 μM CPT for 4 h revealed a translo-

Significance

Histone chaperones are key regulators of transcriptional activity in damaged chromatin regions in the DNA damage response. Here we show that Cc targets the histone chaperone SET/TAF-Iβ in the cell nucleus upon DNA damage, resulting in the blocking of the SET/TAF-Iβ function. Cc is actually translocated into the nuclei of cells treated with a specific DNA damage inducer and not upon death-receptor pathway or stress-induced stimuli. Cc locks the domains engaged in histone binding of SET/TAF-Iβ, inhibiting its nucleosome assembly activity. Structural characterization of the complex between Cc and SET/TAF-Iβ provides a valuable template to design drugs aimed at silencing the oncogenic effect of SET/TAF-Iβ.

Reserved for Publication Footnotes

Submission PDF

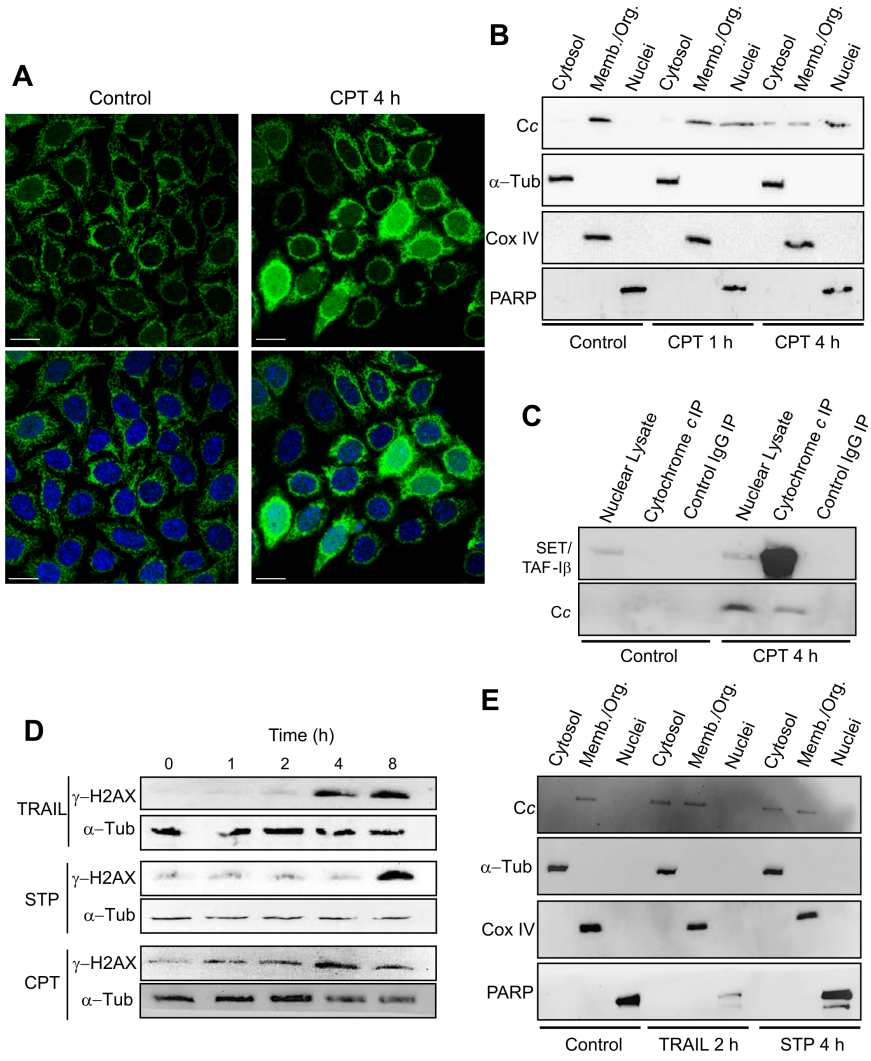

Fig. 1. CPT-induced nuclear translocation of Cc and formation of the Cc:SET/TAF-Iβcomplex.(A) Subcellular localization of Cc-GFP stably expressed (green; upper panel) in Heltog cells upon treatment with 20 μM CPT for 4 h detected by confocal microscopy (x60 oil objective). Nuclei were stained in blue with Hoechst. Co-localization of green Cc-GFP fluorescence and blue nuclear staining is shown in the merge images (lower panel). Scale bars are 25 μm.**(B)** Subcellular fractioning showing Cc location upon treatment with 20 μM CPT for 1 or 4 h. Non-treated and CPT-treated Heltog cells were fractionated to yield cytosolic, membrane/organelle (Memb./Org.) and nuclear fractions. Purity of subcellular fractions was verified by Western blot using anti-α-Tub (50 kDa), anti-Cox IV (17 kDa) and anti-PARP (116 kDa) antibodies.**(C)** IP of SET/TAF-Iβwith Cc after treating Heltog cells with 20 μM CPT for 4 h. Western blot showed the detection of SET/TAF-Iβas a ∼34 kDa band (lanes 1 and 4) in the nuclear fraction. Cc-IP of nuclear lysates from non-treated (lane 2) and CPT-treated cells (lane 5), followed by probing with the SET/TAF-Iβantibody (*upper*). Mouse IgG was used as control (lanes 3 and 6). Confirmation of immunoprecipitated Cc from nuclear lysates is also shown (lanes 4 and 5) under CPT treatment (*lower*).**(D)** DNA-damage response upon treatment of Heltog cell cultures with 100 ng/mL TRAIL, 1 μM STP or 20 μM CPT for 0, 1, 2, 4 and 8 h. Specific antibody against phosphorylated γ-H2AX was used in Western blotting. α−Tub antibody was used as loading control. **(E)** Subcellular fractioning showing Cc location upon treatment with 100 ng/ml TRAIL for 2 h or 1 μM STP for 4 h.

cation of C*c*-GFP from mitochondria to the cytoplasm and the nucleus. The nuclear localization of C*c*-GFP has been confirmed by colocalization with the Hoechst staining (Fig. 1A: right). In addition, subcellular fractionation of Heltog cells treated with 20 μM CPT showed C*c* accumulation in the cell nucleus after 4 h (Fig. 1B). In fact, C*c* appeared in the nucleus after 1 h treatment, as previously observed in HeLa cells treated with either UV irradiation or CPT (20). Co-detection in the nuclear cell fraction with nuclear-specific poly (ADP-ribose) polymerase (PARP) confirmed the C*c* translocation into the nucleus (Fig. 1B).

To further demonstrate the relationship between endogenous SET/TAF-Iβ and C*c* in response to DNA damage, *in cell* interaction between them was examined using immunoprecipitation (IP). An antibody against C*c* was used to extract associated proteins in nuclear lysates of Heltog cells treated with 20 μM CPT for 4 h. As shown in Fig. 1C, SET/TAF-Iβ co-immunoprecipitated with C*c* after CPT treatment (lane 5), while untreated cells (control) did not show any band corresponding to SET/TAF-Iβ (lane 2). To confirm the IP specificity, nuclear lysates from untreated and CPT-treated cells were probed with the SET/TAF-Iβ antibody (Fig. 1C: lanes 1 and 4, respectively), while the negative controls (Fig. 1C: lanes 3 and 6) did not show any band when mouse immunoglobulin G was used. C*c* IP was confirmed by immunoblotting the same membrane with the anti-C*c* antibody (Fig. 1C).

To examine whether the observed C*c*:SET/TAF-Iβ interaction is restricted to cells experiencing DNA damage, the effect of tumour necrosis factor (TNF)-related apoptosis-inducing ligand (TRAIL) and staurosporine (STP) – two well-known apoptosis-inducing agents for which DNA damage is not an initiating event – was studied. TRAIL is a member of the TNF superfamily either by the extrinsic pathway or by the BH3 interacting-domain death agonist (Bid)-mediated mitochondrial pathway (21). STP is a broad-spectrum protein kinase inhibitor that promotes intracellular stress-induced apoptosis (22). Apoptosis induction with TRAIL or STP may result in DNA damage in later stages of treatment. Therefore, cell cultures were first tested to determine whether they exhibited DNA damage following TRAIL- or STP-induced apoptosis. To this end, Heltog cell lysates were treated with 100 ng/ml TRAIL or 1 μM STP for 1, 2, 4 and 8 h and immunoblotted against Ser139-phosphorylated histone H2AX (γ-H2AX). γ-H2AX is an extremely sensitive marker of DNA damage as it accumulates rapidly in response to double-strand breaks (DSBs). As shown, the DNA-damage-dependent accumulation of γ-H2AX occurs after 4 h or 8 h of treatment with TRAIL and STP, respectively (Fig. 1D). By contrast, CPT promotes histone H2AX phosphorylation after 1 h. Since no significant DNA damage was observed following exposure to TRAIL for 2

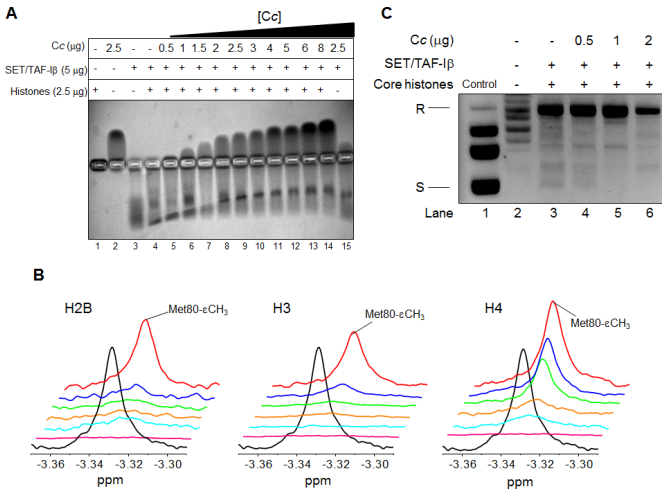

Fig. 2. Competition between histones and Cc for binding to SET/TAF-Iβ.(A) EMSA showing competitive interaction of SET/TAF-Iβwith calf thymus histones in presence of Cc at increasing concentrations. **(B)** 1D ^{1}H NMR spectra monitoring Met-80 methyl signal of reduced Cc in presence of SET/TAF-Iβand *Xenopus laevis* core histones. Details of superimposed 1D ^{1}H NMR spectra of 13 μM reduced Cc (either free [black] or bound to 3.5 μM SET/TAF-Iβ[pink]) in presence of the *Xenopus laevis* core histones H2B, H3 or H4 at increasing concentrations of 5 μg (cyan), 10 μg (orange), 20 μg (green), 30 μg (blue) and 40 μg (red). **(C)** Impairment of the histone chaperone activity of SET/TAF-IβbyCc.2 μg SET/TAF-Iβwas combined with 200 ng relaxed plasmid after being treated with Topo I and incubated with 2 μg HeLa core histones. Nucleosome assembly activity was tested in absence (lane 3) and presence of Cc at increasing concentrations (lanes 4-6). Relaxed and supercoiled forms of circular plasmid DNA are indicated by 'R' and 'S', respectively. Lane 2 corresponds to DNA plasmid relaxed after treatment with Topo I, whereas lane 1 (control) shows supercoiled, untreated DNA plasmid.

h or STP for 4 h, these exposure times were selected to further explore Cc localization. Consequently, following the exposure of Heltog cell cultures to 100 ng/ml TRAIL for 2 h or 1 μM STP for 4 h, subcellular fractionation was applied, indicating Cc as having been translocated from mitochondria to cytosol, but not to the nucleus (Fig. 1E). This corresponds to findings in previous studies of Cc release from mitochondria in response to TRAIL and STP (23, 24). Nevertheless, our study shows Cc as having been unable to reach the cell nucleus following treatments with TRAIL or STP (Fig. 1E). This contrasts with the presence of Cc in the nucleus observed in response to CPT-induced DNA damage (Fig. 1A and B). Altogether, these results indicate that a specific DNA-damage stimulus (CPT) triggers nuclear translocation of Cc, thereby permitting binding to its nuclear target SET/TAF-Iβ.

Cc binds to SET-TAF-Iβ and blocks histone binding

In order to explore the biological significance of the Cc:SET/TAF-Iβ interaction in the cell nucleus in response to a DNA-damage stimulus, we tested the ability of Cc to prevent histone binding to SET/TAF-Iβ. Hence, an electrophoretic mobility shift assay (EMSA) was performed to detect complex formation between SET/TAF-Iβ and calf thymus histones and to further study the effect of the addition of Cc. The mobility of the histone mixture, as well as Cc and SET/TAF-Iβ, are shown in Fig. 2A (lanes 1 to 3). Due to their opposite charges, Cc and SET/TAF-Iβ migrated in reverse directions. The lower mobility of SET/TAF-Iβ following histone addition (Fig. 2A: lane 4) indicates the formation of chaperone-histone complexes. The addition of Cc at increasing concentrations to the SET/TAF-Iβ and histone mixture (Fig. 2A: lanes 5 to 14), made the chaperone mobility match that observed for the Cc:SET/TAF-Iβ complex (lane 15), revealing that Cc competes with histones for the SET/TAF-Iβ binding site.

To confirm the EMSA results, Nuclear Magnetic Resonance (NMR) measurements of reduced Cc were recorded in the presence of SET/TAF-Iβ and *Xenopus laevis* core histones H2B, H3 and H4. The use of isolated core histones allowed for a comparison of their respective binding affinities for the chaperone in competition with Cc. However, binding to core histone H2A could not be tested, as the recombinant expression of H2A was not possible. Specifically, the Met80-εCH_3 NMR signal of the methionine axial ligand of Cc (Met80) was monitored. As shown, this signal broadens beyond the detection limit upon the addition of SET/TAF-Iβ (Fig. 2B). This is due to the long diffusional correlation time of Cc bound to SET/TAF-Iβ, which results in a fast signal relaxation. As expected for a binding competition, titration of the Cc:SET/TAF-Iβ solution with increasing concentrations of H2B, H3 or H4 core histones led to dissociation of Cc from SET/TAF-Iβ and the recovery of the Met80-εCH_3 signal. Circular dichroism (CD) spectra of SET/TAF-Iβ and core histones H2B, H3 and H4 corroborated the proper secondary structure organization of the proteins (Fig. S1).

To compare the binding thermodynamics of the complexes formed by SET/TAF-Iβ with Cc and core histones, Isothermal Titration Calorimetry (ITC) experiments were performed. Measurements revealed the interaction between Cc and SET/TAF-Iβ being slightly exothermic and entropically driven (binding enthalpy, $^{\Delta}$H, -0.9 kcal mol^{-1}) with a dissociation constant (K_D) of 3.1 μM and a Cc:SET/TAF-Iβ stoichiometry of 2:1 at 25 ºC (Table 1). Notably, the binding of Cc to SET/TAF-Iβ exhibited weak positive cooperativity (Fig. S2), yielding a cooperativity constant (k) of 3.8 and leading to a smaller K_D value and a very positive enthalpy of interaction for the second site (Table 1). In other words, the binding of the first Cc molecule increases 3.8 times the affinity for the binding of a second Cc molecule to SET/TAF-Iβ. Cooperativity can be ascribed to direct ligand-ligand interactions or to protein conformational changes. Therefore, it might be plausible that, following the binding of the first Cc molecule, SET/TAF-Iβ undergoes a conformational change that facilitates the interaction with the second Cc molecule.

As before, ITC experiments were used to quantitatively assess the binding of SET/TAF-Iβ to the core histones H2B, H3 and H4 from *Xenopus laevis*. As shown, (Fig. S3, Table 1) H3 binds SET/TAF-Iβ with a lower affinity (K_D = 25 μM) than H2B (K_D = 2 μM) or H4 (K_D = 6 μM). These values agree with those previously reported for the interaction of SET/TAF-Iβ with H2B (K_D = 2.87 μM), but differ slightly for H3 (K_D = 0.15 μM) (25). In all cases, the stoichiometry of histone:SET/TAF-Iβ interactions was 2:1 (Table 1).

The SET/TAF-Iβ histone binding domain is engaged during binding to Cc

Considering that Cc binds to SET/TAF-Iβ and affects its interaction with core histones, we aimed at determining whether Cc recognizes the SET/TAF-Iβ histone-binding domain. SET/TAF-Iβ forms a headphone-shaped homodimer, each monomer consisting of an N-terminus, a backbone helix, an "earmuff" domain and an acidic disordered stretch (5) (Fig. S4). The region of SET/TAF-Iβ responsible for histone binding and chaperone activity comprises the lower area of the so-called "earmuff" domain (5). In order to examine the SET/TAF-Iβ region involved in binding to Cc, two different SET/TAF-Iβ deletion mutants were designed. The first included the N-terminus along with the backbone helix (hereafter referred to as SET/TAF-Iβ$_{(1\text{-}80)}$ [amino acids 1 to 80]), whereas the second (hereafter referred to as SET/TAF-Iβ$_{(81\text{-}277)}$ [amino acids 81 to 277]) encoded the "earmuff" domain and the acidic stretch of the C-terminus. Worth particular mention is that CD spectra of both mutants indicated a secondary structure similar to that of the *wild-type* protein (Fig. S1). ITC of Cc interactions with SET/TAF-Iβ$_{(1\text{-}80)}$ and SET/TAF-Iβ$_{(81\text{-}277)}$ showed the binding reaction in both cases (Fig. S5: upper). However, weak calorimet-

Submitted Manuscript

Table 1. Thermodynamic values inferred from ITC measurements. Thermodynamic equilibrium parameters for the interaction of *wild-type* and mutant SET/TAF-Iβ with Cc, H2B, H3 or H4 core histones. Equilibrium dissociation constant (K_D), enthalpy (△H), entropy (-T△S), Gibbs free energy (△G) and reaction stoichiometry (n) are shown. Protein-protein interaction affinity is defined by Gibbs energy for binding: △G = -RT lnK_A = RT lnK_D. △G has two different contributions, △H and -T△S, according to equation △G = △H - T△S. *Cooperativity parameters (Gibbs energy [△g], enthalpy [△h] entropy [-T△s] and cooperativity constant [*k*]) are indicated for cooperative binding.

Protein complex	△G (kcal mol^{-1})	△H (kcal mol^{-1})	-T△S (kcal mol^{-1})	K_D (μM)	n
Cc:SET/TAF-Iβ	-7.5 (△g -0.8)*	-0.9 (△h 6.1)*	-6.6 (-T△s -6.9)*	3.1 (*k* 3.8)*	2.0
H2B:SET/TAF-Iβ	-7.8	-2.6	-5.2	2.0	2.1
H3:SET/TAF-Iβ	-6.3	-3.9	-2.4	25	2.0
H4:SET/TAF-Iβ	-7.1	-1.4	-5.7	6.0	1.9
Cc:SET/TAF-Iβ$_{(1-80)}$	-5.9	1.9	-7.8	44	0.98
Cc:SET/TAF-Iβ$_{(81-277)}$	-6.8	6.7	-13.5	9.6	0.98
Cc:S162A/K164A/D165A	-7.1	-2.4	-4.7	6.3	1.9
Cc:T191A/T194A/D195A	-6.4	-4.4	-2.0	22	1.9

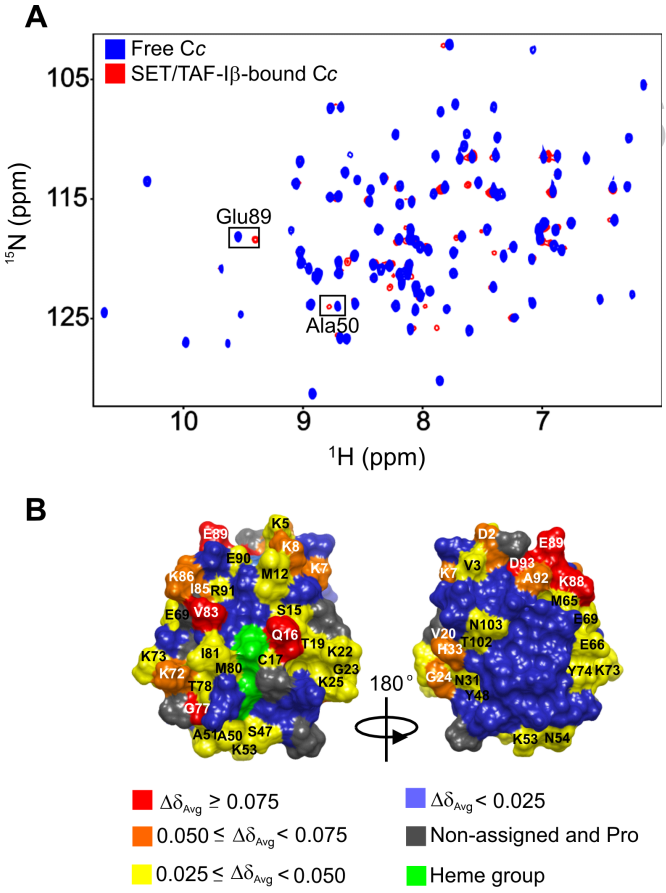

Fig. 3. NMR titrations of ^{15}N-labeled Cc with SET/TAF-Iβ. (A) Superimposed [^{1}H-^{15}N] 2D HSQC spectra of ^{15}N-labeled Cc, which is either free or bound to dimeric SET/TAF-Iβat Cc:SET/TAF-Iβ molar ratio of 1:0.25.**(B)** Mapping of Cc residues perturbed upon binding to SET/TAF-Iβ. Cc surfaces are rotated 180° around vertical axes in each view. Residues are colored according to their △δ_{Avg} (ppm).

ric signals in the thermogram of SET/TAF-Iβ$_{(1-80)}$ throughout the titration with Cc (Fig. S5: upper) suggest a weak interaction with an estimated K_D of 44 μM (Table 1). On the contrary, the affinity between Cc and SET/TAF-Iβ$_{(81-277)}$ was higher and yielded a K_D of 9.6 μM. The results indicate a binding preference of Cc for the C-terminus of SET/TAF-Iβ and explain the way Cc hampers the chaperone's ability to bind to histones.

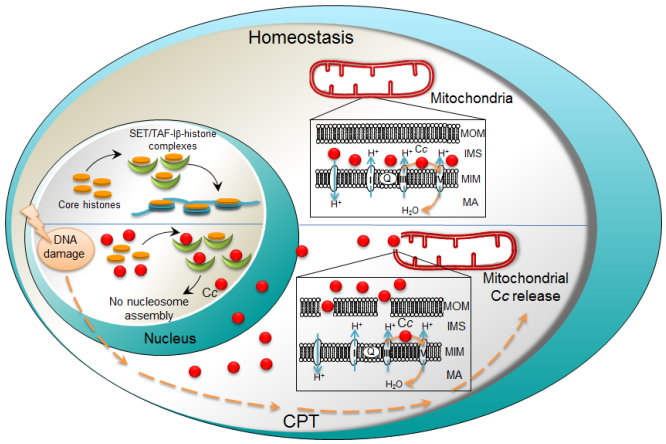

Fig. 4. Figure 4. Proposed model of Cc-mediated nucleosome assembly disability under DNA damage. Schematic assembly of nucleosomes by SET/TAF-Iβunder homeostasis (upper) and its impairment by Cc upon nuclear translocation under DNA damage conditions (lower) both showing: mitochondrial outer membrane (MOM), mitochondrial intermembrane space (IMS), mitochondrial inner membrane (MIM) and matrix (MM).

To further confirm the C-terminus of SET/TAF-Iβ as the region interacting with Cc, two SET/TAF-Iβ mutants were obtained by replacing three adjacent amino acid residues from the "earmuff" domain by alanine residues (Fig. S4). Mutants S162A/K164A/D165A and T191A/T194A/D195A (Fig. S4: green and red, respectively) failed to bind to histones and demonstrated significantly reduced histone chaperone activity (35% of *wild-type* activity) (5). According to the calorimetric data resulting from the titrations of the two SET/TAF-Iβ triple mutants with Cc (Fig. S5: lower panels), the S162A/K164A/D165A mutant shows a higher affinity towards Cc (K_D = 6.3 μM) than T191A/T194A/D195A (K_D = 22 μM). These findings suggest that threonine residues at positions 191 and 194 and aspartate at 195, located in the lower region of the "earmuff" domain, are involved in the interaction with Cc, as they are in the histone remodelling activity of SET/TAF-Iβ.

SET/TAF-Iβ histone chaperone activity is impaired by Cc

As binding to core histones is essential for the histone chaperone activity of SET/TAF-Iβ, the ability (or inability) of Cc to affect such activity was tested using a supercoiling assay (Fig. S6). As shown, SET/TAF-Iβ assembled nucleosomes through the introduction of negative supercoils in the DNA plasmid in the presence of Topoisomerase I (Topo I) and core histones (Fig. 2C: lane 3). Strikingly, the chaperone activity of SET/TAF-Iβ was found to have been impaired following the addition of Cc

in increasing concentrations (Fig. 2C: lane 4 to 6). Controls corresponding to the supercoiling assay in the presence of isolated SET/TAF-Iβ, HeLa core histones, C*c* or a combination are also shown (Fig. S7). Altogether, these findings unequivocally demonstrate that C*c* binds to SET/TAF-Iβ and strongly hinders its ability to function as a histone chaperone.

The Cc heme crevice faces SET/TAF-Iβ upon binding

To dig into the structural features of the interaction between C*c* and SET/TAF-Iβ, the C*c*:SET/TAF-Iβ interaction was monitored by recording [^{1}H, ^{15}N] Heteronuclear Single-Quantum Correlation (HSQC) spectra of fully reduced ^{15}N-labelled C*c*, which was either free or bound to unlabeled SET/TAF-Iβ. Titration of SET/TAF-Iβ onto ^{15}N C*c* resulted in a significant broadening of the C*c* resonances, thereby suggesting the formation of the Cc:SET/TAF-Iβ complex (Fig. 3A). Additionally, specific resonances from residues at the complex interface may show enhanced broadening. Consequently, the line-widths ($^{\triangle\triangle}\nu_{1/2\text{Binding}}$) of ^{15}N-labelled C*c* resonances were analyzed in a pure C*c* sample and a 1:0.25 C*c*:SET/TAF-Iβ mixture . Signals showing this effect corresponded to Thr19, Lys39, Gly41, Gln42, Tyr48, Lys79, Ile81, Ala92 and Leu94 in the ^{15}N dimension (Fig. S8). Hence, these residues can be expected to be at or near the region of C*c* interacting with SET/TAF-Iβ.

In addition to specific line broadening, several amide resonances in the [^{1}H, ^{15}N] HSQC spectra of C*c* exhibit chemical-shift perturbations (CSPs) in the presence of SET/TAF-Iβ (Fig. 3A). For instance, the details of the superimposed spectra (Fig. S9A) shows that Ala50 and Glu89 resonances shift gradually at increasing C*c*:SET/TAF-Iβ ratios (1:0.06, 1:0.12 and 1:0.25). These CSPs indicates that these residues experienced a change in their chemical environment in the presence of SET/TAF-Iβ. Then, they may belong to the complex interface.

In order to identify the residues involved in the complex interface, an average CSP analysis ($^{\triangle}\delta_{\text{Avg}}$) of the C*c* amide signals was obtained. As shown, ^{15}N C*c* resonances from Gln16, Gly77, Val83, Lys88, Glu89 and Asp93 experience significant chemical shifts ($^{\triangle}\delta_{\text{Avg}} \geq 0.075$) following binding to SET/TAF-Iβ (Fig. S9B). Strikingly, residues of ^{15}N C*c* demonstrating CSPs are located on the N- and C- terminus regions on the side of the exposed heme periphery (Fig. 3B).

Notably, a similar surface patch of C*c* is involved in the interactions with cytochrome *c* oxidase (26) and cytochrome bc_1 (27) in the mitochondrial respiratory chain. Interestingly, the interaction between C*c* and the SET/TAF-Iβ chaperone implicated ten lysine residues – namely 5, 7, 8, 22, 25, 53, 72, 73, 86 and 88 (Fig. 3B) – thereby evidencing the key role of electrostatic forces in the formation of C*c*:SET/TAF-Iβ complexes. Similarly, lysine residues are also involved in the interaction with cytochrome bc_1 (27, 28). Given the well-known "lysine masking activity" of SET/TAF-Iβ that prevents the acetylation of histone lysines inside the INHAT complex (3), it is plausible that SET/TAF-Iβ also recognizes the lysine residues from C*c*.

Intriguingly, the C*c* residues thought to play an important role in the interaction between the hemeprotein and apoptosis protease-activating factor-1 (Apaf-1) – namely, Lys7, Lys25, Lys39 and Lys72 (29) – perfectly match those identified in this study as interacting with SET/TAF-Iβ. Furthermore, whereas studies of the complex formed between C*c* and pro-survival protein Bcl-x_L identified both His26 and Gly41 as the most important C*c* residues affected upon binding (30), the present study shows a change only in Gly41 following the addition of SET/TAF-Iβ to the C*c* sample.

A structural look into the Cc:SET/TAF-Iβ complex and NMR-based molecular docking models

With the aim of defining C*c*:SET/TAF-Iβ complex interface regions, NMR restraint-driven docking was performed. CSPs obtained from NMR analysis of the C*c*:SET/TAF-Iβ complex at a 1:0.25 ratio were used as input data. From the 500 solutions obtained from the NMR-based docking for C*c*:SET/TAF-Iβ (Fig. S10A), C*c* geometric centres are represented around Robertson (ribbon) diagrams of SET/TAF-Iβ. In agreement with the two binding sites observed by ITC titrations, the models predicted by the NMR restraint-driven docking yielded two differentiated clusters. One of these clusters included the vast majority of highest scoring models (Fig. S10A: cluster 1), whereas the second cluster encompassed less than 50 solutions (Fig. S10A: cluster 2). Interestingly, nearly all the probe solutions are located in the same region of SET/TAF-Iβ – namely, between its "earmuff" domains. This finding supports the data reported in earlier sections of this study suggesting a C*c* binding preference for the SET/TAF-Iβ histone-binding domain. Indeed, the highest scoring solution from the first cluster revealed how C*c* leans its heme group to approach the lower region of a SET/TAF-Iβ "earmuff" domain (Fig. S10B). The surface representation of both proteins shows them to be in close contact**.** A secondary set of C*c* structures with higher energies (cluster 2) was found near the backbone helices (Fig. S10C).

Discussion

Inefficient repair of DNA lesions results in genome instability, which can, in turn, lead to premature aging and cancer (31). Chromatin dynamics regulate transcriptional activity in response to DNA damage by promoting accessibility to DNA and serving as a docking site for repair and signalling proteins, thereby increasing repair efficiency (8, 32). Recent works reveal how histone chaperones temporarily evict histones from a damaged site in order to facilitate access of repair factors to DNA lesions (9). However, once a DNA break is repaired, histone chaperones return histone proteins to the repaired site (33) and promote the recovery of transcriptional activity (7, 13).

The data presented in this study shows the histone chaperone and oncoprotein SET/TAF-Iβ to specifically interact with C*c* in cell nuclei in response to CPT-induced DNA damage. While translocation of C*c* to the nucleus had previously been observed (19, 20), the specific role of C*c* in the nucleus has yet to be fully elucidated. However, this work shows C*c* translocates into the cell nucleus in response to CPT-induced DNA damage, but not following the TRAIL-activated extrinsic pathway or STP-triggered stress-induced apoptosis. The present study demonstrates that nuclear translocation of C*c* occurs early in the DNA damage response – just one hour after CPT treatment. The finding suggests that C*c* might be imported into the nucleus by diffusion through the nuclear pore complex, although the precise molecular mechanism is as yet unknown. As neither TRAIL nor STP trigger C*c* entry into the cell nucleus, the interaction between C*c* and SET/TAF-Iβ seems to be specifically linked to CPT-induced DNA damage.

CPT selectively targets the essential mammalian enzyme Topo I in nuclei (34). CPT binds covalently to Topo I and supercoiled DNA, thereby forming a ternary complex that inhibits DNA religation and generates a greater number of DSBs (35). Recently, it has been proposed that histone chaperones play a central role as histone carriers in chromatin disassembly connected with DNA repair and transcription recovery following DNA damage (7, 9, 13, 33). Thus, histone chaperones such as HIRA (13), FACT (12), nucleolin (14), APLF (6) Asf1 (9), CAF-1 (10), DAXX (11), p400 (15), NAP1L1 and NAP1L4 (7) actively promote transient chromatin disorganization and histone reshaping in response to DNA damage (8). Since SET/TAF-Iβ belongs to the NAP1 family, it is tempting to hypothesize a role – similar to that described for the above mentioned histone chaperones – for SET/TAF-Iβ in chromatin reshaping in response to DNA

Submission PDF

lesions. Such a role would also explain the C*c*-mediated inhibition observed here.

The results of ITC and NMR titrations performed in the present study reveal the oncoprotein SET/TAF-Iβ as binding specifically to C*c*. Interestingly, C*c* uses the surface residues surrounding its heme group to interact with the histone chaperone, as it does with its respiratory partners cytochrome *c* oxidase (26) and cytochrome bc_1 (27), and its apoptotic partner Apaf-1 (29).

Mutagenesis and NMR-based docking analysis carried out here demonstrated that C*c* docks between the two histone binding domains of SET/TAF-Iβ, thereby preventing the binding of the latter to core histones. Therefore, and as inferred from nucleosome assembly activity assays, it may be concluded that C*c* not only binds to SET/TAF-Iβ, but also hampers the latter's histone chaperone activity. It may therefore be proposed that, following DNA damage induced by CPT, the translocation of C*c* into the cell nucleus and resulting core histone displacement may hinder SET/TAF-Iβ nucleosome assembly activity (Fig. 4). Thus, the specific inhibition of SET/TAF-Iβ by C*c* could contribute not only to the suppression of the former's normal chaperone activity when apoptosis is inevitable and such activity is no longer necessary, but also to obstruct nucleosome remodelling that follows DNA damage repair.

Our finding that C*c* interacts with the oncoprotein SET/TAF-Iβ upon its release from mitochondria suggests that the role of C*c* in the execution of apoptosis is wider than previously held, insofar as it goes beyond caspase cascade activation, by also inhibiting pro-survival C*c* partners. To our knowledge, the SET/TAF-Iβ oncoprotein is indeed the first C*c* target in the nucleus to be identified either in homeostasis or during apoptosis. The results presented not only reveal the molecular basis for the blocking of SET/TAF-Iβ activity by C*c*, but also suggest that the inhibition of this oncoprotein could be a promising objective in the development of anti-cancer drugs. More specifically, an understanding of the molecular interfaces in the complex formed by SET/TAF-Iβ □and its inhibitor, C*c*, could facilitate the development of new drugs aimed at silencing the oncogenic effect of SET/TAF-Iβ histone chaperone activity.

Material and Methods

Expression and purification protocols of C*c*, *wild-type* SET/TAF-Iβ, SET/TAF-$Iβ_{(1-80)}$, SET/TAF-$Iβ_{(81-277)}$, mutants S162A/K164A/D165A and T191A/T194A/D195A, and *Xenopus laevis* core histones H2B, H3 and H4 are described in SI Materials and Methods. Experimental details of apoptosis induction, subcellular fractionation, Western blot analysis, IP, ITC, EMSA, CD, NMR, nucleosome assembly assays and molecular docking calculations are likewise described in SI Materials and Methods.

Acknowledgements.

The authors wish to thank Dr Cristina Muñoz-Pinedo (Bellvitge Biomedical Research Institute, Spain) for providing the HeLa Cc-GFP (Heltog) cell line, as well as Dr Masami Horikoshi (University of Tokyo, Japan) for their kind gift of plasmids encoding SET/TAF-Iβ S162A/K164A/D165A and T191A/T194A/D195A mutants. Plasmids encoding four core histones H2A, H2B, H3 and H4 of *Xenopus laevis* were provided by Dr Tim Richmond (Institute of Molecular Biology and Biophysics, Switzerland). We would also like to thank to Dr Encarnación Zafra and Dr Manuel Angulo for their assistance with NMR data collection (Research Centre in Information Technologies [CITIUS], University of Seville) and to the Biointeractomics Platform (cicCartuja, Seville). The authors are grateful to the Spanish Ministry of Economy and Competitiveness (BFU2012-31670, BFU2010-19451, BFU2013-47064-P, SAF2012-32824, RD12/0036/0026) and the European Community through the regional development funding program (FEDER), the Regional Government of Andalusia (BIO198) and the Ramon Areces Foundation for their financial support. We thank Dr Sergio G. Bartual for critical reading of the manuscript. Additional thanks must be given for financial support in the form of access to the Bio-NMR Research Infrastructure co-funded under the 7th Framework Programme of the EC (FP7/2007–2013) grant agreement 261863 and project contract RII3-026145.

Submissions Only

1. Estanyol JM, *et al.* (1999) The protein SET regulates the inhibitory effect of p21Cip1 on cyclin E-cyclin-dependent kinase 2 activity. *J Biol Chem* 274(46):33161-33165.
2. Fan Z, Beresford PJ, Oh DY, Zhang D, Lieberman J (2003) Tumor suppressor NM23-H1 is a granzyme A-activated DNase during CTL-mediated apoptosis, and the nucleosome assembly protein SET is its inhibitor. *Cell* 112(5):659-672.
3. Seo Sb, *et al.* (2002) Regulation of histone acetylation and transcription by nuclear protein pp32, a subunit of the INHAT complex. *J Biol Chem* 277(16):14005-14010.
4. Okuwaki M, Nagata K (1998) Template activating factor-I remodels the chromatin structure and stimulates transcription from the chromatin template. *J Biol Chem* 273(51):34511-34518.
5. Muto S, *et al.* (2007) Relationship between the structure of SET/TAF-Iβ/INHAT and its histone chaperone activity. *Proc Natl Acad Sci USA* 104(11):4285-4290.
6. Mehrotra PV, *et al.* (2011) DNA repair factor APLF is a histone chaperone. *Mol Cell* 41(1):46-55.
7. Cho I, Tsai P-F, Lake RJ, Basheer A, Fan H-Y (2013) ATP-dependent chromatin remodeling by cockayne syndrome protein B and NAP1-like histone chaperones is required for efficient transcription-coupled DNA repair. *PLoS Genet* 9(4):e1003407.
8. Adam S, Polo SE (2014) Blurring the line between the DNA damage response and transcription: The importance of chromatin dynamics. *Exp Cell Res* 329(1):148-153.
9. Tanae K, Horiuchi T, Matsuo Y, Katayama S, Kawamukai M (2012) Histone chaperone Asf1 plays an essential role in maintaining genomic stability in fission yeast. *PLoS ONE* 7(1):e30472.
10. Polo SE, Roche D, Almouzni G (2006) New histone incorporation marks sites of UV repair in human cells. *Cell* 127(3):481-493.
11. Lacoste N, *et al.* (2014) Mislocalization of the centromeric histone variant CenH3/CENP-A in human cells depends on the chaperone DAXX. *Mol Cell* 53(4):631-644.
12. Dinant C, *et al.* (2013) Enhanced chromatin dynamics by FACT promotes transcriptional restart after UV-induced DNA damage. *Mol Cell* 51(4):469-479.
13. Adam S, Polo SE, Almouzni G (2013) Transcription recovery after DNA damage requires chromatin priming by the H3.3 histone chaperone HIRA. *Cell* 155(1):94-106.
14. Kobayashi J, *et al.* (2012) Nucleolin participates in DNA double-strand break-induced damage response through MDC1-dependent pathway. *PLoS ONE* 7(11):e49245.
15. Xu Y, *et al.* (2012) Histone H2A.Z controls a critical chromatin remodeling step required for DNA double-strand break repair. *Mol Cell* 48(5):723-733.
16. Kalousi A, *et al.* (2015) The Nuclear oncogene SET controls DNA repair by KAP1 and HP1 retention to chromatin. *Cell Rep* 11(1):149-163.
17. Martínez-Fábregas J, *et al.* (2014) Structural and functional analysis of novel human cytochrome *c* targets in apoptosis. *Mol Cell Proteomics* 13(6):1439-1456.
18. Martinez-Fabregas J, Diaz-Moreno I, Gonzalez-Arzola K, Diaz-Quintana A, & De la Rosa MA (2014) A common signalosome for programmed cell death in humans and plants. *Cell Death Dis* 5:e1314.
19. Zhao S, Aviles ER, Fujikawa DG (2010) Nuclear translocation of mitochondrial cytochrome *c*, lysosomal cathepsins B and D, and three other death-promoting proteins within the first 60 minutes of generalized seizures. *J Neurosci Res* 88(8):1727-1737.
20. Nur-E-Kamal A, *et al.* (2004) Nuclear translocation of cytochrome *c* during apoptosis. *J Biol Chem* 279(24):24911-24914.
21. Gonzalvez F, Ashkenazi A (2010) New insights into apoptosis signaling by Apo2L/TRAIL. *Oncogene* 29(34):4752-4765.
22. Feng G, Kaplowitz N (2002) Mechanism of staurosporine-induced apoptosis in murine hepatocytes. *Am J Physiol Gastrointest Liver Physiol* 282(5):G825-G834.
23. Sarker M, Ruiz-Ruiz C, López-Rivas A (2001) Activation of protein kinase C inhibits TRAIL-induced caspases activation, mitochondrial events and apoptosis in a human leukemic T cell line. *Cell Death Differ* 8(2): 172-181
24. Johansson AC, Steen H, Ollinger K, & Roberg K (2003) Cathepsin D mediates cytochrome *c* release and caspase activation in human fibroblast apoptosis induced by staurosporine. *Cell Death Differ* 10(11):1253-1259.
25. Karetsou Z, *et al.* (2009) Identification of distinct SET/TAF-Iβ domains required for core histone binding and quantitative characterisation of the interaction. *BMC Biochem* 10(1):10.
26. Sakamoto K, *et al.* (2011) NMR basis for interprotein electron transfer gating between cytochrome *c* and cytochrome *c* oxidase. *Proc Natl Acad Sci USA* 108(30):12271-12276.
27. Moreno-Beltrán B, *et al.* (2014) Cytochrome c_1 exhibits two binding sites for cytochrome *c* in plants. *Biochim. Biophys. Acta-Bioenerg.* 1837(10):1717-1729.
28. König BW, *et al.* (1980) Mapping of the interaction domain for purified cytochrome c_1 on cytochrome *c*. *FEBS Lett* 111(2):395-398.
29. Yu T, Wang X, Purring-Koch C, Wei Y, McLendon GL (2001) A mutational epitope for cytochrome *c* binding to the apoptosis protease activation factor-1. *J Biol Chem* 276(16):13034-13038.
30. Bertini I, Chevance S, Del Conte R, Lalli D, Turano P (2011) The anti-apoptotic Bcl-$_{XL}$ protein, a new piece in the puzzle of cytochrome *c* interactome. *PLoS ONE* 6(4):e18329.
31. Insinga A, Cicalese A, Pelicci PG (2014) DNA damage response in adult stem cells. *Blood Cell Mol Dis* 52(4):147-151.
32. Lavelle C, Foray N (2014) Chromatin structure and radiation-induced DNA damage: From structural biology to radiobiology. *Int J Biochem Cell Biol* 49:84-97.
33. Ransom M, Dennehey BK, Tyler JK (2010) Chaperoning histones during DNA replication and repair. *Cell* 140(2):183-195.
34. Liu LF, *et al.* (2000) Mechanism of action of camptothecin. *Ann N Y Acad Sci* 922(1):1-10.
35. Jacob S (2005) Effects of camptothecin on double-strand break repair by non-homologous end-joining in DNA mismatch repair-deficient human colorectal cancer cell lines. *Nucleic Acids Res* 33(1):106-113.

Please review all the figures in this paginated PDF and check if the figure size is appropriate to allow reading of the text in the figure.

If readability needs to be improved then resize the figure again in 'Figure sizing' interface of Article Sizing Tool.